Sorption of Sulfate and Chloride Anions on a Well-Characterized Al 2024 Electrode

A. Kolics, J. C. Polkinghorne, A. E. Thomas,† and A. Wieckowski*

Department of Chemistry and Frederick Seitz Materials Research Laboratory, University of Illinois at Urbana−Champaign, 600 South Mathews Avenue, Urbana, Illinois 61801

Received September 3, 1997. Revised Manuscript Received December 9, 1997

We studied sorption processes, adsorption and incorporation, of sulfate and chloride anions on the surface of well-characterized aluminum 2024 alloy using electrochemical, radiochemical, and ultrahigh−vacuum spectroscopic techniques. The measurements were carried out at an open-circuit potential and in the electrode potential range on the negative side of the open-circuit potential (cathodic polarization conditions), at various pH values. The focus was on sorption reversibility as well as on the relationship between anion's surface concentration and the electrode potential. We have found that sorption of sulfate anion is controlled by pH, surface charge, and the stability of aluminum oxide films. We have also found that adsorption of chloride is weaker than sulfate and is more irreversible since chloride incorporation occurs more readily than sulfate. The change in the alloy surface composition and morphology induced by the electrochemical treatment and anion adsorption was monitored by scanning Auger microscopy and energy-dispersive X-ray spectroscopy. The characterization exhibits copper-rich *intrusions* and *extrusions* that may act as either local cathodes or anodes in the overall alloy dissolution process. The distribution and evolution of such Cu-rich inclusions under studied experimental conditions were monitored and are reported. The dissolution of aluminum from the alloy affects both sulfate and chloride adsorption/incorporation processes. While sulfate and chloride adsorption have no effect on cathodic current measured in the studied electrode potential range, the high anion surface concentration may have a detrimental effect on the alloy stability, particularly when the beneficial influence of the cathodic polarization (protection) ends.

Introduction

Adsorption or incorporation of anions from aqueous media on base metals and alloys frequently occurs under both laboratory and industrial conditions and may lead to passive film degradation through pitting and crevice corrosion. Conversely, such sorption processes may contribute to corrosion inhibition.[1−3] A systematic study of anion adsorption and incorporation may help in better understanding and, ultimately, improving control of aluminum corrosion. Our recent approach has been to use electrochemical and in situ radioactive labeling techniques to investigate surface interactions of anions with such substrates as stainless steel and aluminum[4−6] and, preliminarily with the Al 2024 alloy.[6,7] The alloy, in the focus of these investigations, owns a widespread technological application due to its high strength and low density. Unfortunately, these advantageous mechanical properties are accompanied by poor alloy resistance toward intergranular corrosion and stress corrosion cracking.[8,9]

The alloying element that is responsible for the localized corrosion susceptibility of the Al 2024 alloy is copper.[9−15] Despite a broad body of scientific information in support of this assertion, there is only a limited insight into the copper behavior in the aluminum matrixes, particularly during cathodic polarization. The knowledge of the cathodic behavior that exists stems from observations related to an increasing use of aluminum alloys in offshore applications where the cathodic protection under immersed conditions may become necessary for prolonged service life.[16] We have

* Corresponding author.
† Present address: Eastman Kodak Co., Research and Development Laboratories, 1609 Lake Avenue, Rochester, NY 14650.

(1) Nguyen, T. H.; Foley, R. T. *J. Electrochem. Soc.* **1980**, *127*, 2563.
(2) Mansfeld, F.; Kendig, M. W.; Lorenz, W. J. *J. Electrochem. Soc.* **1985**, *132*, 290.
(3) McCafferty, E. *J. Electrochem. Soc.* **1990**, *137*, 3731.
(4) Thomas, A. E.; Sung, Y.-E.; Gamboa-Aldéco, M.; Franaszczuk, K.; Wieckowski, A. *J. Electrochem. Soc.* **1995**, *142*, 476.
(5) Thomas, A. E.; Kolics, A.; Wieckowski, A. *J. Electrochem. Soc.* **1997**, *144*, 586.
(6) Kolics, A.; Thomas, A. E.; Wieckowski, A. *Langmuir* **1995**, *11*, 4605.
(7) Kolics, A.; Thomas, A. E.; Wieckowski, A. In *New Techniques for Characterizing Corrosion and Stress Corrosion*; Jones, R. H., Baer, D. R., Eds.; TMS Publication: Warrendale, PA, 1996; p 247.
(8) Galvele, J. R.; de Micheli, S. M.; Muller, I. L.; de Wexler, S. B.; Alanis, I. L. Localized Corrosion, NACE, 1979; pp 580−599.
(9) Kaesche, H. Localized Corrosion, NACE, 1979; pp 516−525.
(10) Saito, A.; Latanision, R. M. In *International Congress on Metallic Corrosion*; Toronto, Canada, June 3−7, 1984; Proceedings, Vol. 3, pp 122−129.
(11) Zahavi, J.; Rotel, M.; Huang, H.-C. W.; Totta, P. A. International Congress on Metallic Corrosion, Toronto, Canada, June 3−7, 1984; Proceedings, Vol. 2, pp 311−316.
(12) Mazurkiewicz, B.; Piotrowski, A. *Corrs. Sci.* **1983**, *23*, 697.
(13) Rota, A.; Böhni, H. *Werkstoffe Korros.* **1989**, *40*, 219; **1989**, *40*, 295.
(14) Scully, J. R.; Frankenthal, R. P.; Hanson, K. J.; Siconolfi, D. J.; Sinclair, J. D. *J. Electrochem. Soc.* **1990**, *137*, 1365; **1990**, *137*, 1373.
(15) Chen, G. S.; Gao, M.; Wei, R. P. *Corrosion* **1996**, *52*, 8.

S0897-4756(97)00603-0 CCC: $15.00
Published on Web 02/10/1998

already reported a strong influence of copper on the cathodic part of the polarization curve of Al 2024[6] and provide evidence as to adsorption of sulfate on the surface of the alloy. In this work, we elaborate mechanistic details of the sorption processes, including the incorporation, and extend the measurements to chloride[17] under otherwise identical experimental conditions. These comprehensive investigations, also carried out with pure aluminum, demonstrate a significant difference in the sorption behavior between the two popular anions, sulfate and chloride, that are always present in environmental or industrial settings. The surface analytical studies in ultrahigh vacuum (UHV), in parallel with the in situ measurements, furnish information on the morphological rearrangements and chemical changes that occur simultaneously with the anion sorption processes. While it is well-known that the electrochemical properties of copper-rich intermetallics and the anion tendency to adsorb on the alloy surface are key factors in controlling the local corrosion of the 2024 alloy, this is the first study attempting to reveal interdependencies, or a synergy, between these properties in the cathodic corrosion of the alloy.

Adsorption time, solution pH, anion bulk concentration, and the electrode potential were the variables of this research. Except in the study of bulk solution pH effects, the solution pH was usually set to be either 3.0 or 11.0. The pH value of 3.0 was chosen since it closely resembles the pH for an accelerated corrosion test of Al 2024 in an offshore environment.[18] On the other hand, the effect of alkaline exposure on the interfacial properties of the alloy is also of importance since an alkaline environment develops beneath the disbonding organic coatings. We also investigated kinetics of surface/bulk exchange between adsorbed (radiolabeled) and solution anions and made use of the progress-of-exchange versus time profiles to gauge the extent of anion incorporation into passive films. Information on surface and substrate-depth distribution of the anionic adsorbates and on surface morphological features was obtained using scanning Auger microscopy (SAM), X-ray photoelectron spectroscopy (XPS), and scanning electron microscopy (SEM). In some instances, electrolytic solutions were analyzed by inductively coupled plasma (ICP). The plan of the paper is such that first the surface characterization of Al 2024 prior to solution exposure is reported. Then, analyses of the solution-treated samples, first by the in situ approach (radiochemistry, electrochemistry, and ICP) and then by the ex situ UHV spectroscopies, are presented. The data obtained under open-circuit potential conditions and the structural/morphological data are discussed first; this is followed by an analysis of a more complex case involving electrode polarization. Adding the UHV spectroscopic part to the in situ research brought the presented research closer to the practice of electrochemistry with well-characterized systems in the category of surface reactivity and materials stability. Although the average properties of the studied interfaces are displayed by the in situ examination and mainly local, microscopic details are provided by the UHV work, these two programs are complementary by yielding a realistic assessment of the surface composition during the sorption events investigated. In other words, the spectral data provide a backbone for interpretation of the radiochemical and electrochemical results on adsorption and incorporation of anions that are the main focus of this study.

Experimental Section

The working electrodes were made of a technological Al 2024-T3 alloy[19] of the following composition: Si 0.50%, Fe 0.50%, Cu 3.8−4.9%, Mn 0.30−0.9%, Mg 1.2−1.8%, Cr 0.10%, Zn 0.25%, Ti 0.15%, Al balance; and of pure (99.999%) aluminum. Samples of 0.6 cm^2 geometric surface area were used. Prior to the experiments, a chosen electrode was wet polished with SiC emery paper down to #4000 and washed with Millipore water. Unless called "as-received" in Results, the electrode was introduced into the measuring cell for electrochemical characterization and anion adsorption. The Ag/AgCl ($[Cl^-] = 3$ M) half-cell and a thin gold wire were used as reference and counter electrodes, respectively. All potentials quoted in this paper are given versus this reference electrode, which is 0.20 V negative to the standard hydrogen electrode (SHE). The cathodic polarization was always started from a stable open-circuit potential (OCP) value. The OCP was attained within 2 h after the electrode immersion into the solution and reached a value between −0.60 and −0.90 V, depending on the solution pH and sulfate concentration conditions.

To conduct the radioactive labeling experiments, sodium sulfate (ICN) and sodium chloride (ICN) labeled with ^{35}S and ^{36}Cl, respectively, were used. The molar activities of the radioactive stock solutions were 1.11 TBq/mol (^{35}S) and 17.3 GBq/mol (^{36}Cl). The radioactive labeling technique, the calculation of surface concentration values, and other experimental conditions are as previously reported.[4,6,7] Average standard deviations in Γ values were ±11% and ±15% in the experiments with ^{35}S and ^{36}Cl, respectively.

Solution pH was adjusted by either perchloric acid or sodium hydroxide addition. Oxygen-free nitrogen was used to purge all solutions and to create an inert gas blanket during the experiments. Wherever necessary, the bulk concentration of aluminum, iron, and copper obtained from Al 2024 dissolution was measured by a Perkin-Elmer (Norwalk, CT), 2000 dual inductively coupled plasma (ICP) spectrophotometer. The aluminum, iron, and copper concentrations of the blank were taken to determine the minimum detectable amounts. After correcting for the signals from the blank samples, the detection limits were 0.170, 0.020, and 0.006 ppm for aluminum, copper, and iron, respectively.

Ultrahigh-vacuum (UHV) measurements were conducted using a Physical Electronic Industries PHI Model 660 AES spectrometer and a Physical Electronic Industries PHI Model 5400 XPS spectrometer. In SAM studies, a 10 keV electron beam energy with emission current of 40 nA were applied. XPS analysis were performed at a 25° takeoff angle with respect to the surface plane. A Mg Kα source (1250 eV) was employed for all studies at a beam voltage of 15 kV at 400 W. The analyzed area was 3.5 mm^2. The samples used in the UHV program were pretreated in the same manner as those in electrochemical or radioactive labeling experiments except that polishing was continued down to 1 μm with diamond paste in order to minimize surface roughening effects in the spectroscopic analysis. Prior to the XPS analysis, the sample was immersed in Millipore water for 10 s to avoid the formation of sodium perchlorate crystals on the surface. After the brief immersion, the sample was transferred to the UHV instrument while being protected by a hanging water drop to reduce exposure of the surface to ambient upon system evacuation.

(16) Gundersen, R.; Nisancioglu, K. *Corrosion* **1990**, *46*, 279.
(17) Kolics, A.; Thomas, A. E.; Wieckowski, A. *J. Chem. Soc., Faraday Trans.* **1996**, *92*, 3727.
(18) Tankins, E.; Kozol, J.; Lee, E. W. *JOM* **1995**, *47*, 40.
(19) Jones, D. In *Principles and Prevention of Corrosion*; MacMillan Publishing Co.: New York, 1992.

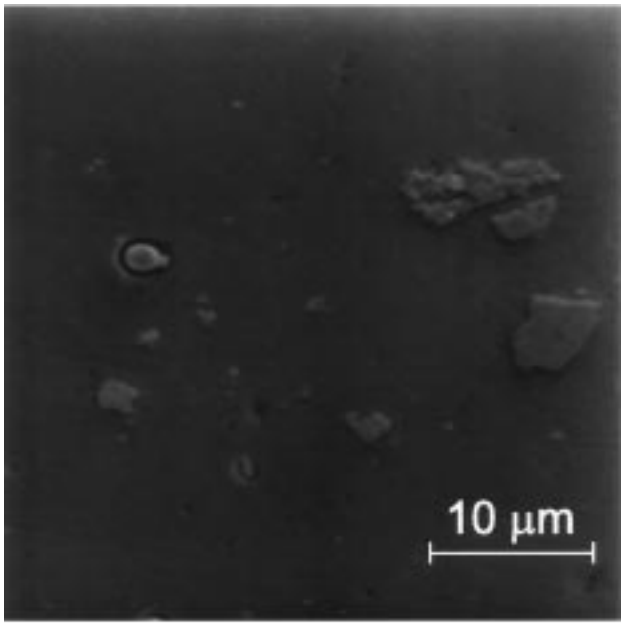

Figure 1. Scanning electron microscopy image of Al 2024 surface after wet polishing.

Scanning electron microscopy measurements were performed using a Hitachi S-800 microscope equipped with a field emission electron gun (accelerator voltage was 20 keV). The sample was tilted to 30° with respect to the analyzer for both imaging and qualitative/quantitative analyses. Other parameters and experimental conditions are as commonly employed in scanning electron microscopy measurements.

The roughness of the Al 2024 samples was analyzed by a Dektak 3ST surface profiler (Veeco/Sloan Technology). In each case, seven line scans of 1.5 mm in length with 250 nm horizontal and 1 nm vertical resolution were used. From this experiment, the average roughness of the sample, which is the average height deviation from the middle line, is determined.

Results

I. Surface Characterization Al 2024 before Solution Exposure. Scanning electron microscopy (SEM) and energy-dispersive analysis by X-ray spectroscopy (EDAX) analyses were performed to provide information on the substrate surface morphology and composition prior to solution exposure. The micrographs indicate that the surface is not homogeneous, and reveal the presence of surface heterogeneities of either an *intrusion* or *extrusion* type (Figure 1). The intrusions are generally round-shaped and are surrounded by a ditch that is indicative of an enhanced substrate dissolution around the particle. Intrusions are generally 1−4 μm in size and have a surface density of approximately $(0.5-1.5) \times 10^5$ intrusions cm^{-2}. Extrusions have no characteristic shapes and are not surrounded by such enhanced dissolution zones. There are small (<0.3 μm) and large (3−20 μm) extrusions with a surface density of $(1-4) \times 10^8$ extrusions cm^{-2} and $(1-5) \times 10^5$ extrusions cm^{-2}, respectively. EDAX data taken to identify the bulk composition of the heterogeneities, as well as the composition of the homogeneous parts of the surface, are presented in Figure 2. On the homogeneous parts, aluminum, small amounts of copper, trace amounts of manganese, and magnesium are present. Intrusions contain aluminum, copper, and magnesium while the extrusions are composed of aluminum, copper, iron, and manganese. Only these two types of the intermetallic particles were found on the surface. The bulk composition of these surface heterogeneities varied from experiment to experiment, which does not warrant a strictly quantitative treatment. The data would support, however, the presence of $CuMgAl_2$ and $CuMnFeAl_6$ intermetallics that are known to be a part of the Al 2024 alloy.[10,12,15] Notably, it is already known that these surface heterogeneities differ in their electrochemical behavior; $CuMnFeAl_6$ may serve only as a local cathode while $CuMgAl_2$ can be both a local cathode or an anode, as the anodic and cathodic exchange current density on the $CuMgAl_2$ intermetallics is higher than on aluminum.[10]

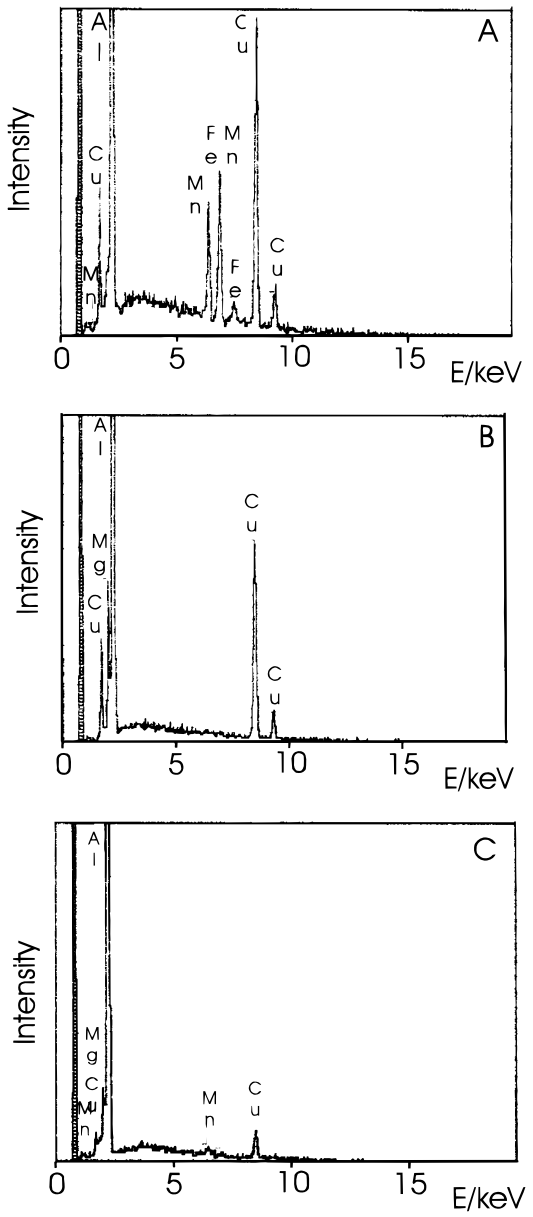

Figure 2. Energy-dispersive analysis by X-ray spectroscopy analysis of the composition of extrusions (A), intrusions (B), and the homogeneous part of Al 2024 (C), after the Al 2024 electrode emersion from 0.1 M $NaClO_4$ + 1 mM Na_2SO_4 solution at pH = 3.0 under open-circuit conditions.

We also performed a comparative analysis of these intermetallics by Auger electron spectroscopy. This technique has a sampling depth of a few atomic layers in contrast to EDAX analysis that samples much deeper

(micrometer range). Such parallel experiments provide information on the surface and bulk distribution of the intermetallic components. AES analysis indicated that there was magnesium depletion and copper enrichment in the surface layer of $CuMgAl_2$. One possible reason for such arrangement of copper and magnesium is that magnesium may selectively dissolve from the $CuMgAl_2$ intermetallics during wet polishing,[20] leaving a copper-enriched surface layer. The top surface layer of the other intermetallic phase, $CuFeMnAl_6$, showed copper and iron enrichment and manganese depletion as compared to the bulk composition.

II. Open-Circuit Potential Measurements. *1. Sorption of Sulfate and Chloride.* At open-circuit potential (OCP), where the surface is not affected by the electrode polarization, sorption of sulfate is relatively fast and a steady-state surface concentration is established within 5 min (Figure 3A). The relatively high amount of sulfate accumulated on the substrate surface, despite high perchlorate ion concentration in the electrolyte, provides evidence for strong interactions between the sulfate anion and the oxidized surface of the alloy.[21−23] Such interactions are characteristic of a specific adsorption or an incorporation of the anions.[24] As shown in Figure 3B, sulfate coverage is pH dependent; the surface concentration, or coverage, passes through a maximum at pH = 2.0 and systematically decreases with an increase in pH.

Not only sorption of sulfate but also that of chloride is a relatively fast surface process (Figure 4A). In acidic and neutral solution, chloride surface concentration is significantly smaller than that of sulfate and is also less affected by solution pH (Figure 4B). The data confirm previous assessments that chloride is weakly bonded to the oxide surfaces in acidic media.[21−23,24]

A solution concentration dependence of the sulfate surface concentration was mreasured in 0.1 M $NaClO_4$ at pH = 3.0. The rate of sulfate deposition is not significantly influenced by the solution concentration of sulfate (Figure 5), leading us to believe that the ion migration through a surface film or across the surface and/or competitive desorption of water molecules from the surface are the rate-controlling steps. The surface concentration increases as the logarithm of the sulfate concentration in the solution. This is probably a nonisotherm behavior since sulfate adsorption, to a large extent, is accompanied by the incorporation of sulfate in the oxide layer (see below).

It is also important to know whether the sulfate surface concentration may exceed a monolayer coverage. Assuming that sulfate adsorbs on surface hydroxyl groups of aluminum, the number of OH groups should determine the maximum surface concentration. Although much data are available on surface hydroxyl groups on aluminum surfaces,[25−28] the estimates of

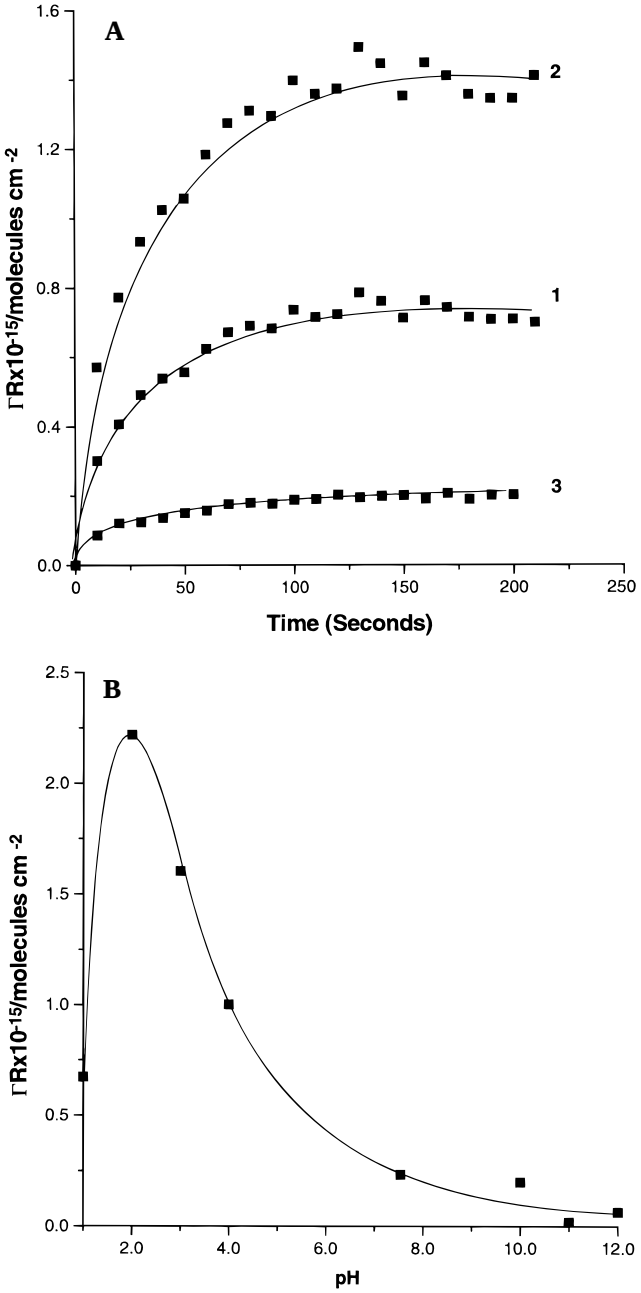

Figure 3. Radioactive labeling data. (A) Time dependence of sulfate sorption on the Al 2024 surface in 0.1 M $NaClO_4$ at pH = 1.0 (curve 1), pH = 3.0 (curve 2), and pH = 10.0 (curve 3). $c_{sulfate}$ = 0.1 mM. (B) Sorption of sulfate on the Al 2024 surface as a function of solution pH. $c_{sulfate}$ = 0.1 mM.

surface concentrations of such groups differ by more than an order of magnitude and range from 0.6×10^{14} to 9×10^{14} OH groups cm^{-2}. Assuming that the roughness factor (R) of our electrodes is 3[4,17] and using 9×10^{14} OH groups cm^{-2} as the highest estimate, the maximum number of monolayer sulfate ions (attached to the OH groups via bidentate bonding[21]) would be 1.35×10^{15} ions cm^{-2} of the real surface. The 1.35×10^{15} ions cm^{-2} value is exceeded by our experimental data at (and above) 0.1 mM and gives evidence as to a

(20) Al-Odan, M. A.; Smyrl, W. H. *J. Electrochem. Soc.* **1997**, *144*, L282.
(21) Rajan, S. S. S. *Soil Sci. Soc. Am. J.* **1978**, *42*, 39.
(22) Rakotonarivo, E.; Bottero, J. Y.; Thomas, F.; Poirier, J. E.; Cases, J. M. *Colloids Surf.* **1988**, *33*, 191.
(23) Kosmulski, M. *Colloids Surf.* **1995**, *95*, 81.
(24) Thomas, Y.-E.; Sung, H. S.; Kim; Wieckowski, A. *J. Phys. Chem.* **1996**, *100*, 11726.
(25) Corey, R. B. In *Adsorption of Inorganics at Solid-Liquid Interfaces*; Anderson, M. A., Rubin, A. J., Eds.; Ann Arbor Science Publishers, Inc.: Ann Arbor, MI, 1981; p 161.
(26) Hohl, H.; Stumm, M. *J. Colloid Interface Sci.* **1976**, *55*, 281.
(27) Wood, R.; Fornasiero, D.; Ralston, J. *Colloids Surf.* **1990**, *51*, 389.
(28) Laiti, E.; Öhman, L. O.; Nordin, J.; Sjöberg, S. *J. Colloid Interface Sci.* **1995**, *175*, 230.

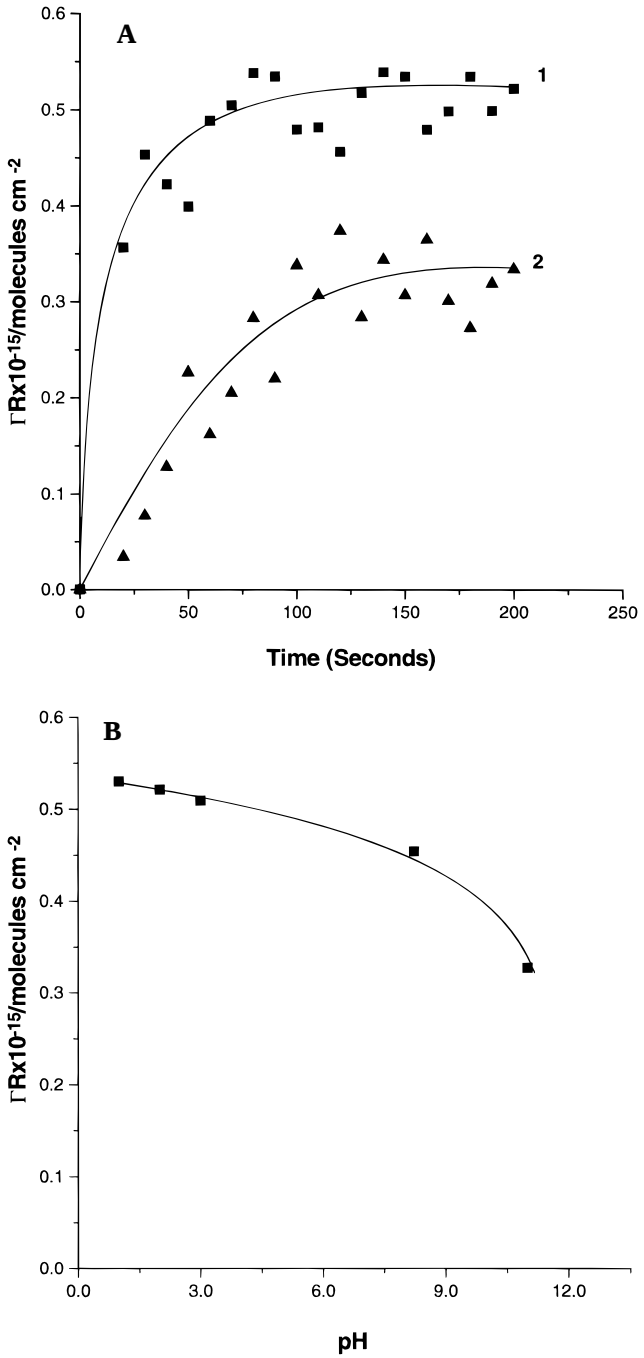

Figure 4. Radioactive labeling data. (A) Time dependence of chloride sorption on Al 2024 in 0.1 M $NaClO_4$ at pH = 3.0 (curve 1) and pH = 11.0 (curve 2). $c_{chloride}$ = 1 mM. (B) Sorption of chloride on Al 2024 as a function of solution pH. $c_{chloride}$ = 1 mM.

multilayer surface process, evidently due to both adsorption and incorporation. For chloride, under the assumption of a monodentate bond between chloride and surface hydroxyl groups,[8] we calculate a surface concentration of 2.7×10^{15} ions cm^{-2}. The latter value is significantly larger than the measured surface concentration (Figure 4B), thus providing further evidence on the different sorption behavior between sulfate and chloride. While chloride coverage is smaller than that of sulfate, it is significantly larger than expected on the basis of pure electrostatic interactions.[23,25] This is in accord with our notion that besides adsorption, the incorporation of chloride into the oxide film takes place

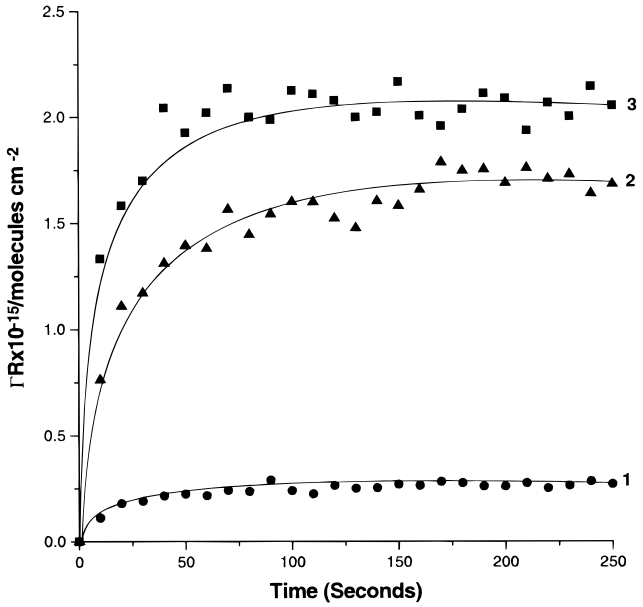

Figure 5. Radioactive labeling data. Time dependence of sulfate sorption on Al 2024 in 0.1 M $NaClO_4$ at different sulfate concentrations at pH = 3.0 under open-circuit conditions. Curve 1: $c_{sulfate}$ = 0.03 mM; curve 2: $c_{sulfate}$ = 0.1 mM; curve 3: $c_{sulfate}$ = 3 mM.

and accounts for the excess chloride coverage. We note that sulfate coverage on pure aluminum remains practically the same as on Al 2024 at pH values between 1 and 12.[29] These results indicate that intermetallics have no influence on the extent of anion adsorption under open-circuit conditions.

The radiochemical method employed for this project[17] is well suited to study the exchange process of a labeled adsorbate present on the electrode surface with the same but unlabeled adsorbate present in the bulk solution. The results of such an experiment provide information on the exchange rate and can be used as a useful criterion of adsorption reversibility. For instance, if the flow of the anions between the surface and the bulk of solution is sufficiently facile, a dilution of radiolabeled surface anions by nonlabeled anions would readily occur, causing a reduction in the count rate from the surface. Using this concept, we studied the exchange of labeled anions present on the surface with the unlabeled anions added to solution in a 10-fold excess (Figure 6). The data show that the sulfate adsorbate exhibits higher mobility toward the exchange process than chloride. Another observation is that the addition of unlabeled chloride at OCP does not influence the surface coverage of the labeled sulfate;[7] this confirms other results showing that the type of surface attachment is different between the two anions.

2. Stability of Al 2024 versus the Solution pH. A major event that accompanies the anion deposition is the dissolution of aluminum and other alloying components from the Al 2024 substrate. Therefore, we studied the stability of Al 2024 in the same pH ranges as highlighted above. The ICP data for aluminum, presented in Figure 7, indicate that the extent of dissolution increases with a decrease in pH below pH = 4.0 and with an increase in pH above pH = 10.0 (not shown).

(29) Kolics, A.; Polkinghorne, J. C.; Wieckowski, A. *Electrochim. Acta*, in press.

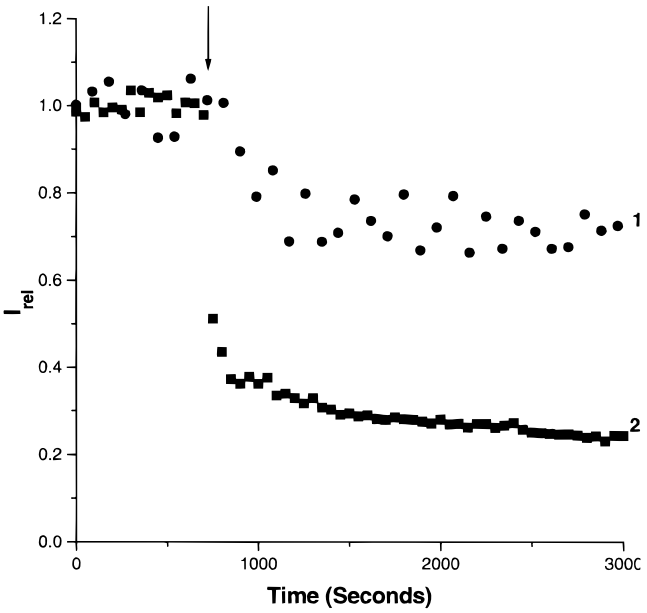

Figure 6. Radioactive labeling data. Exchange of labeled chloride (curve 1) and sulfate (curve 2) deposited on Al 2024 in 0.1 M $NaClO_4$ at pH = 3.0 under open-circuit conditions by the addition of 0.01 M unlabeled sulfate and 0.1 M unlabeled chloride (see text). Initial concentrations of the labeled anions: $c_{sulfate} = 0.1$ mM; $c_{chloride} = 1$ mM.

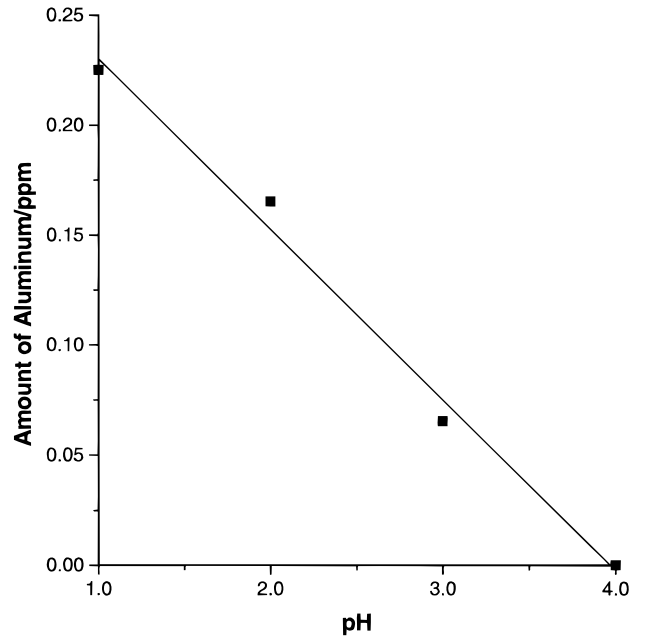

Figure 7. Inductively coupled plasma data. The amount of aluminum dissolved from Al 2024 alloy as a function of pH in 0.1 M $NaClO_4$ + 1 mM Na_2SO_4 under open-circuit conditions.

Iron is present in the solution, although its concentration is practically independent of pH. In contrast to aluminum and iron, no copper dissolution was found in these ICP assays.

3. Composition of the Al 2024 Surfaces. We applied X-ray photoelectron spectroscopy and Auger electron spectroscopy to provide more information on the surface obtained by the Al 2024 substrate exposure to solutions of interest. The XPS data were taken at a 25° takeoff angle after holding the samples under open-circuit conditions at pH = 3.0 and 11.0. After exposure to 0.1 M $NaClO_4$ + 1 mM Na_2SO_4 solution for 30 min, the XPS data taken at 25° revealed sulfate as the only sulfur compound in the oxide film. Our results therefore support previous claims that sulfate is not reduced on/in the oxide film under open-circuit potential conditions.[30] In good agreement with the radiochemical results presented above (cf. with data in Figure 1B), the sulfate content of the oxide film decreases with pH and, at pH = 3.0, is equal to 2.5%, much higher than in alkaline solution, 0.2%. Furthermore, it is found that the relative atomic concentration of sulfate does not change with the takeoff angle between 15° and 45°, which is a clear indication for sulfate incorporation into the oxide film. Despite the high perchlorate concentration in the supporting electrolyte, at pH = 3.0, we found only 0.7% perchlorate in the oxide layer, indicating a higher adsorption strength of sulfate versus that of perchlorate. The sodium content of the oxide is higher at pH = 11.0 (3.3%) than at pH = 3.0 (0.3%) which is most probably due to the deposition of sodium ions on the negatively charged oxide surface. Above pH = 10.0, the surface roughens and the number of extrusions significantly increases. For instance, the average roughness of the surface was 21 and 62 nm after holding the electrode for 30 minutes in pH = 3.0 and 11.0 solutions, respectively. This is due to the selective dissolution of aluminum in alkaline solution.[31] In support of the radiochemical and XPS data, no sulfate was detected on the surface by AES in such high pH solutions.

To provide local information on the top few atomic layers on Al 2024, the samples exposed to 0.1 M $NaClO_4$ + 1 mM Na_2SO_4 at pH = 3.0 were also analyzed by scanning Auger microscopy (SAM). The elemental mapping data confirm that the surface is highly heterogeneous (Figure 8). The surface layers of the intermetallics (intrusions and extrusions) are rich in copper but depleted in aluminum and oxygen versus the homogeneous parts of the surface (Figure 8B−D). The SAM analysis also discloses a unique surface distribution of adsorbed sulfate (Figure 8F). The distribution is spatially uncorrelated to intrusions or extrusions, but the sulfate enrichment is arranged as narrow bands oriented in a preferred direction (see the brightest features in Figure 8F). Although the origin of this unique distribution pattern is not clear, the SAM maps suggest that sulfate distribution occurs along subgrain boundaries.[32,33] In contrast to Al 2024, we found that the surface distribution of sulfate on pure aluminum was homogeneous. Clearly, the heterogeneous structure of Al 2024 has a profound effect on the sulfate alignment on the surface.

III. Polarization Curves versus the State of the Electrode Surface. The polarization curves taken at 0.2 mV s^{-1} (Figures 9) serve as a background for the discussing and interpreting the radiochemical results presented below. In pH < 10 solutions, and on the negative side of the corrosion potential, E_{corr} (Figure 9), the polarization curve can be divided into three sections:[31] (i) hydrogen ion reduction under activation control,

(30) Moshier, C. W.; Davis, G. D.; Ahearn, J. S. *Corros. Sci.* **1987**, *27*, 785.
(31) Kaesche, H. Metallic Corrosion, NACE, Houston, TX, 1985.
(32) Buchheit, R. G.; Moran, J. P.; Stoner, G. E. *Corrosion* **1990**, *46*, 610.
(33) Buchheit, R. G.; Moran, J. P.; Stoner, G. E. *Corrosion* **1994**, *50*, 120.

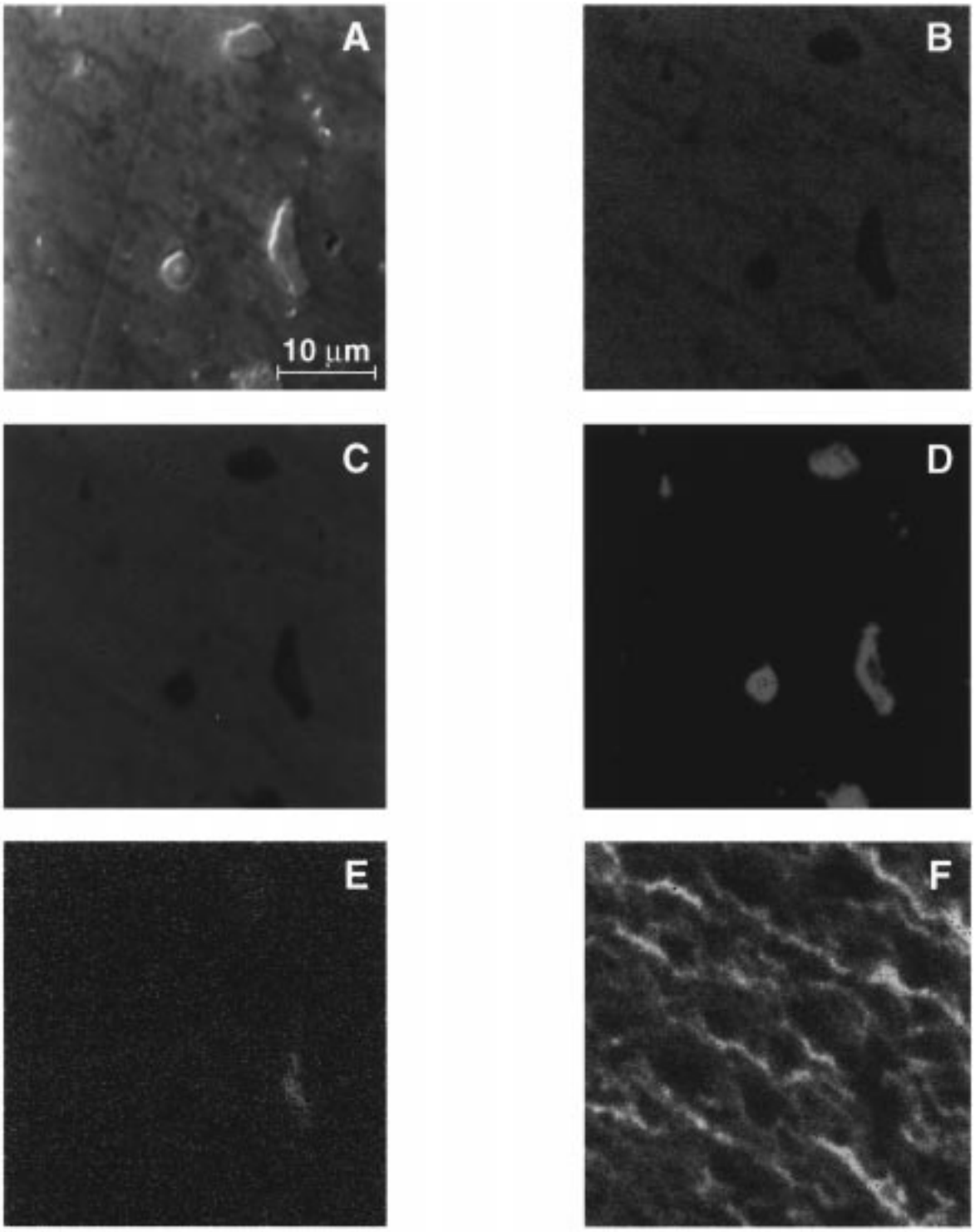

Figure 8. Scanning electron microscopy and scanning Auger microscopy analyses of Al 2024 surface exposed to 0.1 M $NaClO_4$ + 1 mM Na_2SO_4 solution at pH = 3.0 under open-circuit conditions. Presented are (A) SEM image. (B−F) elemental maps, where B corresponds to aluminum, C to oxygen, D to copper, E to iron, and F to sulfur.

(ii) H_3O^+ reduction in the diffusion-limiting region, and (iii) hydrogen evolution through water decomposition process. Due to the low H^+ concentration in pH = 10.0 solution, only the latter process is observable. The addition of sulfate to solution does not have a significant effect on the current-potential profiles as expected from some previous reports.[34]

Morphological and chemical changes induced by cathodic polarization were examined by scanning electron microscopy (SEM) and EDAX. At −1.20 V and pH = 3.0, the SEM data indicate that the surface density of the copper-rich intermetallics significantly increased versus the density obtained under open-circuit conditions (Figure 10A). These intermetallics are surrounded by some brighter areas, which are indicative of an enhanced alloy dissolution. In these experiments we found that the aluminum-depleted bands disappeared,

(34) Van de Ven, E. P. G. T.; Koelmans, H. *J. Electrochem. Soc.* **1976**, *123*, 143.

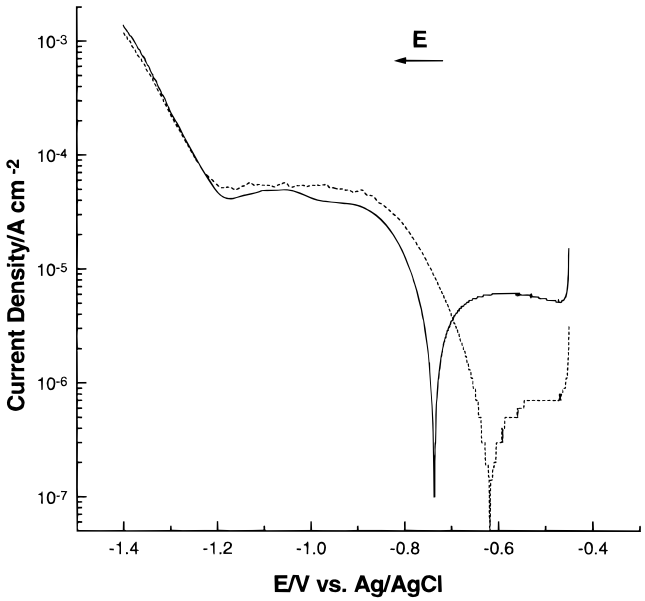

Figure 9. Cathodic polarization curves of Al 2024 in 0.1 M $NaClO_4$ at pH = 3.0 in the absence (—) and presence of 0.1 mM Na_2SO_4 (···). Sweep rate: 0.2 mV s^{-1}.

and the distribution of aluminum (Figure 10B) was more homogeneous than observed under open-circuit conditions. Most importantly, the polarization to −1.20 V induces a major change in the distribution of sulfate on the surface. Instead of the sulfate alignment being unaffected by the presence of the heterogeneities at open-circuit potential, there is now (Figure 10D) a remarkable agglomeration of adsorbed/incorporated sulfate at the intermetallic domains of the surface.

Further polarization of the Al 2024 alloy to −1.40 V causes formation of cracks on the surface (Figure 11A). The emergence of the cracks is most probably due to the hydrogen evolution that destabilizes and ultimately breaks the covering oxide film. Interestingly, copper is now enriched in the cracks and depleted in extrusions (Figure 11D). In contrast to the Al 2024 samples pretreated under open-circuit conditions, we found a homogeneous distribution of aluminum (Figure 11B), most probably due to deposition of aluminum hydroxide on the surface (see Discussion). We also found that sulfate is much more homogeneously distributed at −1.40 V than −1.20 V (Figure 11E). Despite the presence of sulfate on the surface during cathodic polarization (Figures 10D and 11E), no influence of sulfate on either the surface composition or morphology was found. Parallel measurements carried out by EDAX showed (Figure 12) that down to −1.0 V, the amount of copper in the upper layer of Al 2024 is the same as in the bulk of the substrate (see Experimental Conditions). However, during the negative-going polarization below −1.10 V, the copper content increased linearly with an increase in negative potential. The EDAX results indicate that due to the selective dissolution of aluminum, aluminum depletion and copper enrichment extend several micrometers deep into the sample.

The effective presence of intermetallics on the electrochemical behavior of Al 2024 is also demonstrated by the comparison of the cathodic polarization curves of Al 2024 and pure aluminum (Figure 13). The higher current density obtained for Al 2024 (solid line) indicates that the copper-rich intermetallics offer efficient cathodic sites. Therefore, the Al 2024 alloy exhibits a lower overpotential for hydrogen evolution and a more positive corrosion potential than on pure Al. In accord with the surface analytical data, we again conclude that the hydrogen evolution at Al 2024 proceeds predominantly on the intermetallics rather than on pure aluminum.[31,35,36]

IV. Deposition of Sulfate under Electrode Potential Control. *1. pH and Bulk Concentration Dependence.* We may now compare the polarization data from electrochemistry and the sorption data from the radiochemical measurements. [The data plotted in Γ vs *E* curves shown in Figures 14 and 16 are the average of 10 min measurement at the corresponding potential; thus they do not necessarily represent the equilibrium values.] The surface concentration−electrode potential (Γ vs *E*) plots for sulfate at pH = 3.0 are given in Figure 14. The amount of sulfate deposit decreases with the electrode potential down to −1.00 V, then increases and maximizes at −1.20 V. However, further negative polarization induces a strong sulfate deposition. This behavior differs from the results obtained in pure aluminum under very similar experimental conditions where the surface concentration decreased with potential.[6] In contrast to fast anion deposition under the open-circuit conditions (Figure 3A), a sluggish sulfate deposition was observed at −1.10 and −1.20 V (see below). In more acidic media, the amount of sulfate deposition increases with more negative values of the electrode potential (curve 1 in Figure 14), while above pH = 3.0 the sulfate anion is desorbed with an increase in the negative potential (curves 3 and 4 in Figure 14).

2. Dynamic Aspects. A survey of adsorption/desorption kinetics of sulfate anion is given in Figure 15. The applied potential program consisted of a stepwise potential change from −0.70 V to a given potential in the range from −1.10 to −1.40 V. We found that there was a reduction in sulfate surface concentration after each potential step. The decrease was the smallest for the step to −1.10 V and the largest for −1.40 V. After a short induction period at −1.10 V, the amount of surface sulfate increased with time with a slope of 0.9×10^{12} ions cm^{-2} s^{-1}. At −1.20 V, the induction period is shorter and is followed by a strong sulfate deposition at a rate of 2.25×10^{12} ions cm^{-2} s^{-1}. In the studied time interval, no steady-state value was attained; in fact, the sorption continuously increased even after 1 h (not shown). These data indicate that there is an ongoing formation of new surface sites on which the anion adsorbs. On the contrary, at −1.30 V, surface concentration of the sulfate anion sharply decreases at the experiment beginning and then decreases and becomes stable until the end of the measurement. At −1.40 V, after 50 s, the near-complete sulfate desorption is followed by its partial readsorption.

3. Chloride Deposition under Electrode Potential Control. The surface concentration of chloride is sig-

(35) Pourbaix, M. *Atlas of Electrochemical Equilibria in Aqueous Solutions*, 1st English ed.; Pergamon Press: Oxford, 1966.
(36) Malachesky, P. A. In *Encyclopedia of Electrochemistry of the Elements*; Bard, A. J., Ed.; Marcel Dekker, Inc.: New York, 1976; Vol. VI, p 63.

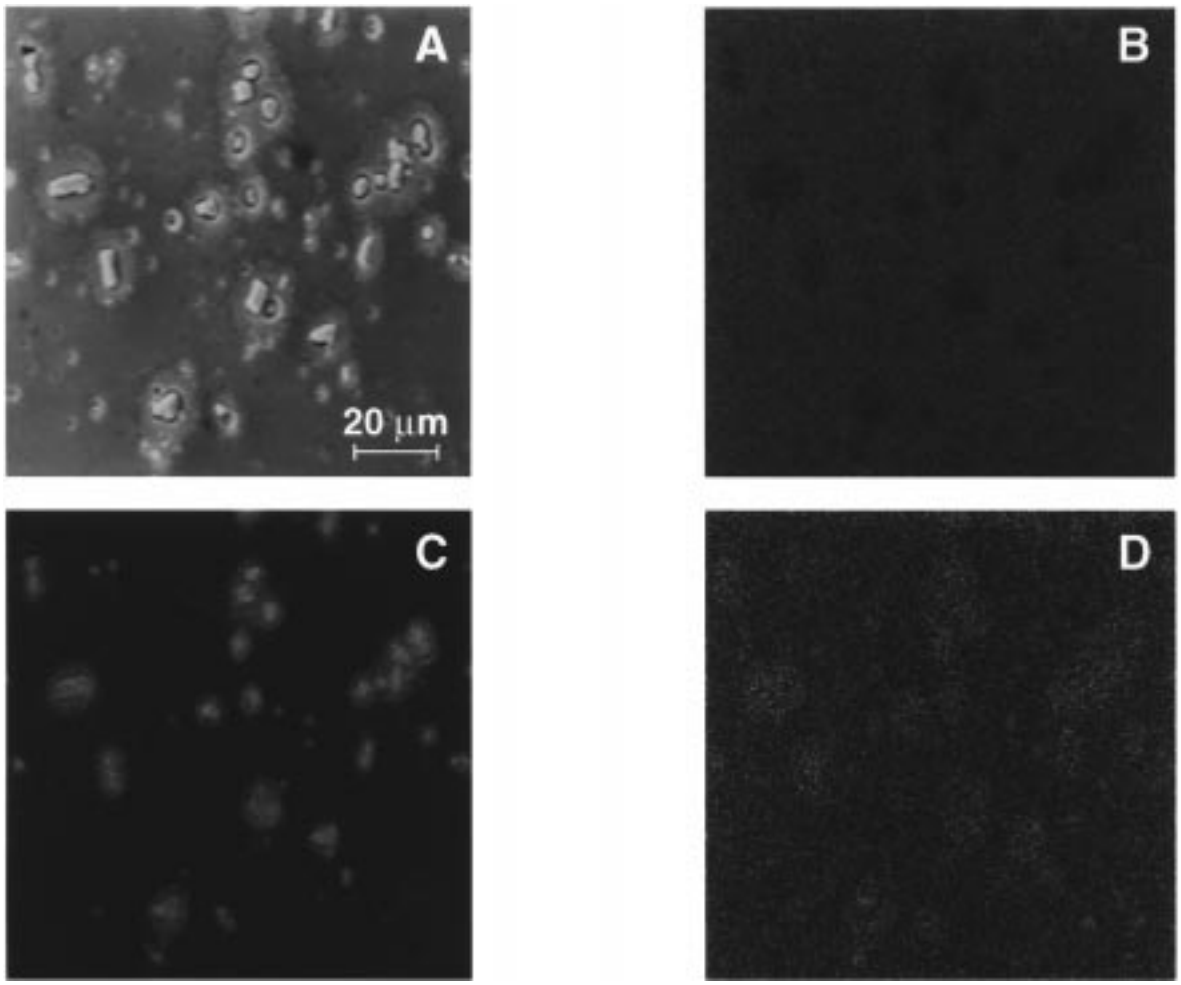

Figure 10. Scanning electron microscopy and scanning Auger microscopy analyses of the Al 2024 surface exposed to 0.1 M $NaClO_4$ + 1 mM Na_2SO_4 solution at pH = 3.0 and at $E = -1.20$ V. (A) SEM image. (B−D) Elemental maps, where B corresponds to aluminum, C to copper, and D to sulfur.

nificantly smaller than that of sulfate in the cathodic potential region (Figure 16). Unlike sulfate, chloride surface concentration is electrode potential independent down to −0.90 V. Next, the sorption of chloride maximizes at −1.00 V then decreases with potential. In a clear analogy to surface sulfate behavior reported above in the potential range from −1.0 to −1.20 V, the surface concentration of chloride is non-steady-state and increases with time (not shown). At −1.40 V, a significant part of the irreversibly accumulated chloride was removed due to the destabilization of the surface oxides into which chloride was entrapped. We also note that in contrast to the small uptake of chloride during cathodic polarization, the anodic polarization enhances chloride deposition which is quite high even after the passive film breakdown.[7]

Discussion

1. Anion Adsorption. The results of the radiochemical exchange measurements (Figure 6) and the data from XPS and AES (Figure 8F) demonstrate that the uptake of sulfate and chloride is a result of simultaneous adsorption on, and incorporation into, the oxide film on Al 2024. The amount of the nonremovable labeled anions involved in the exchange process may be assumed to be proportional to the extent of the anion incorporated into the oxide film, that is, to the anion surface immobility. Therefore, we conclude that chloride mainly migrates into the oxide layer (is then less mobile) while sulfate mainly adsorbs at the oxide/solution interface. More quantitatively,[37,38] using the mobility argument, we may conclude that up to 70% of surface chloride and only 25% of surface sulfate are incorporated in the oxide layer.

We also conclude from the radiochemical and UHV data that solution pH plays a major role in sulfate sorption/alloy dissolution processes (Figures 3, 4, and 7). Using our present and previous results,[21,25−28] we may attempt to formulate a model of sulfate (and chloride) *adsorption*. In a broad range of pH change, from pH = 2.0 to 10.0, a major factor contributing to sulfate *adsorption* (Figure 3) is the charge state of surface hydroxyl groups. The pH of the potential of zero charge (PZC) for aluminum oxides/hydroxides is between 6.0 and 9.0, and in acidic solution, the accumulation of $Al-OH_2^+$ species is accounted for by the surface charge.[23−25] Outside of the potential of zero charge, the charged surface sites electrostatically attract the anions from solution. The experimental formula between sulfate surface concentration and solution pH is de-

(37) Boloanca, Z.; Korelic, O.; Lovrecek, B. *Surf. Technol.* **1984**, *22*, 323.
(38) Lohrengel, M. M. *Mater. Sci. Eng.* **1993**, *R11*, 243, and references therein.

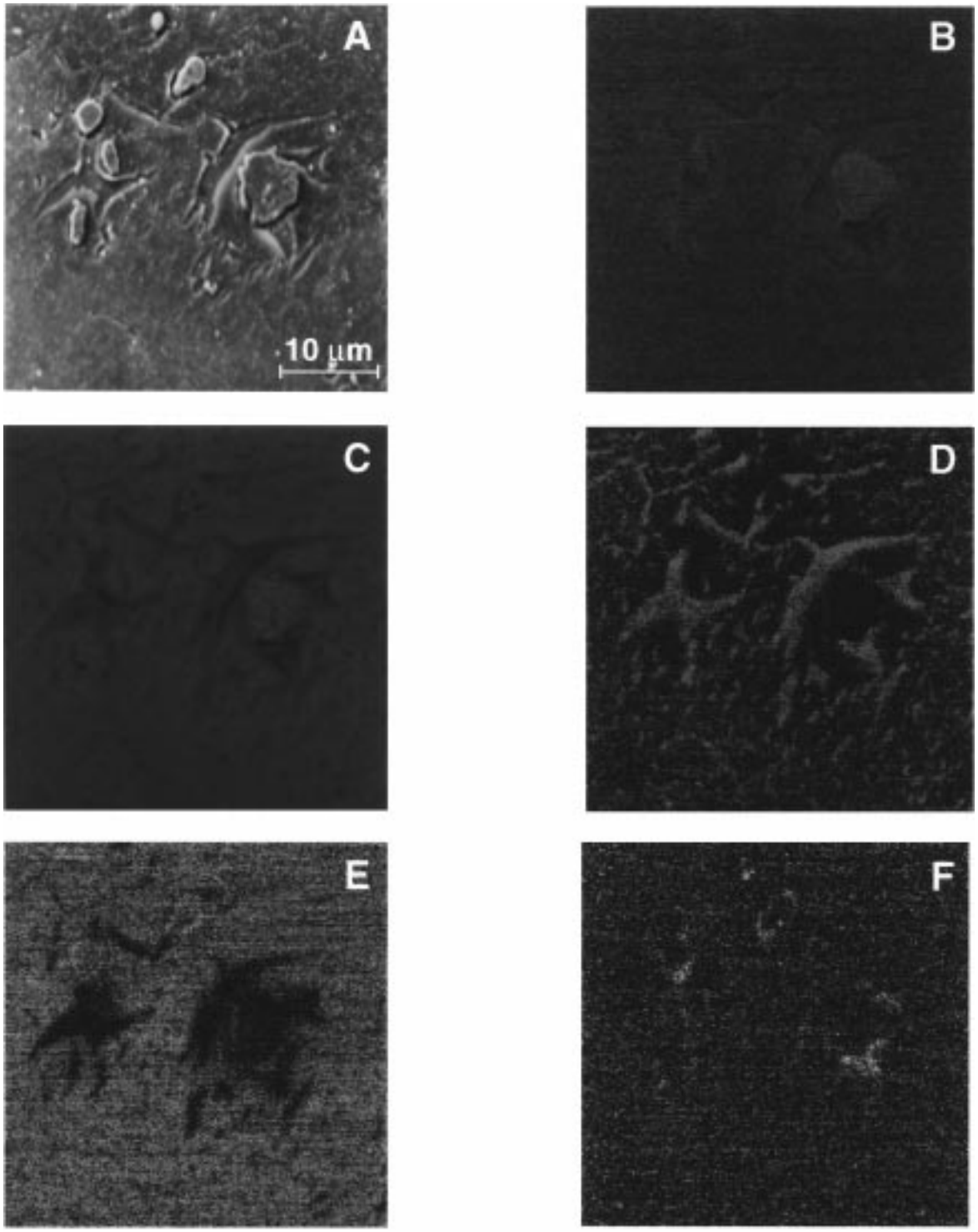

Figure 11. Scanning electron microscopy and scanning Auger microscopy analyses of the Al 2024 surface exposed to 0.1 M $NaClO_4$ + 1 mM Na_2SO_4 solution at pH = 3.0 and at $E = -1.40$ V. (A) SEM image. (B−F) Elemental maps, where B corresponds to aluminum, C to oxygen, D to copper, E to magnesium, and F to sulfur.

scribed by $\log \Gamma R = 15.684 - 0.166\text{pH}$. Such a relationship, when observed, has been interpreted as evidence that the extent of anion adsorption is proportional to the number of positively charged surfaces species.[39] However, sulfate adsorption on $Al-OH_2^+$ also has a chemical component as it gives rise to a monolayer coverage in an electrolyte containing perchlorate anions in 1000-fold excess over the sulfate anions (see below). We conclude that strong contribution to the binding comes from a ligand-exchange process on the $Al-OH_2^+$ sites, as previously demonstrated in studies of sulfate interactions with aluminum and iron oxide *colloids*.[21,40,41] Coincidentally, chloride adsorption on oxide surfaces is known to be controlled by solution pH.[23,25] However, perchlorate ions strongly compete with chloride ions for

(39) Vujicic, V.; Lovrecek, B. *Surf. Technol.* **1982**, *17*, 29.

(40) Hingston, R. J.; Posner, A. M.; Quirk, J. P. *J. Soil Sci.* **1972**, *23*, 177.

(41) Sigg, L.; Stumm, W. *Colloids Surf.* **1981**, *2*, 101.

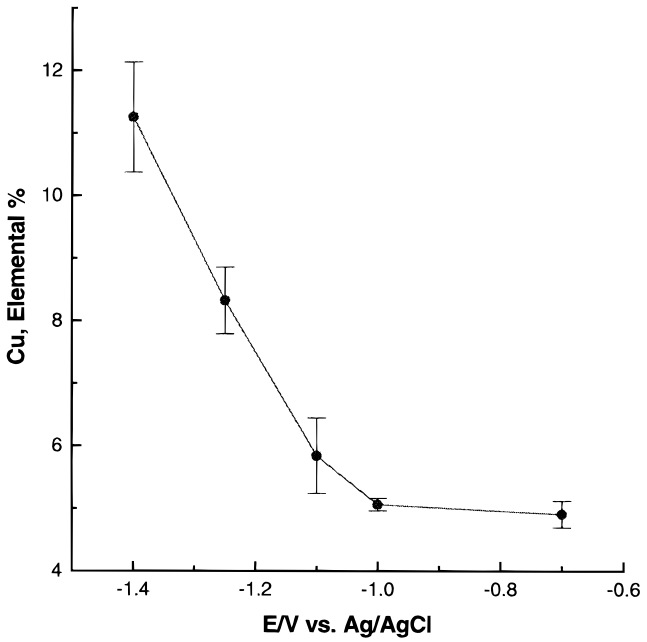

Figure 12. Energy-dispersive analysis by X-ray spectroscopy measurements. Change in copper concentration on the Al 2024 surface during cathodic polarization in 0.1 M $NaClO_4$ at pH = 3.0.

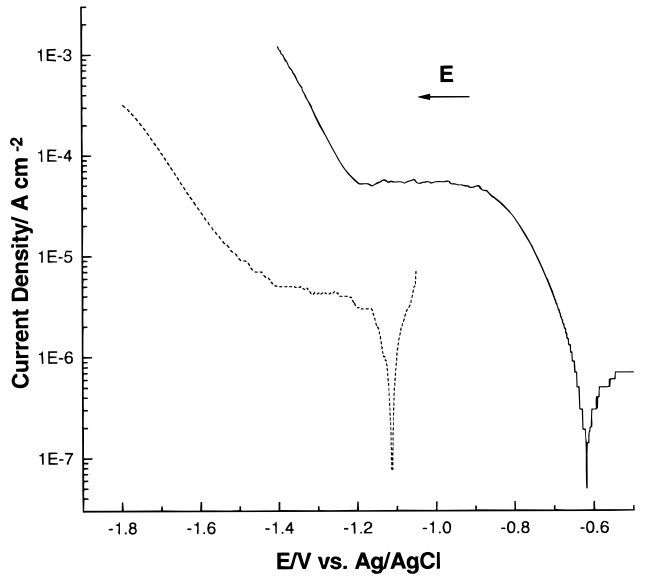

Figure 13. Cathodic polarization curve of the Al 2024 electrode (—) and of an aluminum electrode (•••) in 0.1 M $NaClO_4$ at pH = 3.0. Sweep rate: 0.2 mV s^{-2}.

the surface adsorption sites and suppress chloride adsorption. Overall, the data presented above support the notion that chloride−aluminum−oxide interactions are weak as expected from results obtained on aluminum oxide colloids.[23,25] The strong suppression of chloride in the presence of perchlorate and the high extent of chloride incorporation are reasons for the less pH dependent chloride surface concentration versus that of sulfate.

2. Morphological Data. The electrode polarization dramatically changes the substrate surface morphology and affects the anion adsorption. The shift of the electrode potential from the open-circuit potential value of the cathodic direction causes an enhanced aluminum dissolution around the Cu-rich centers (Figure 10B).

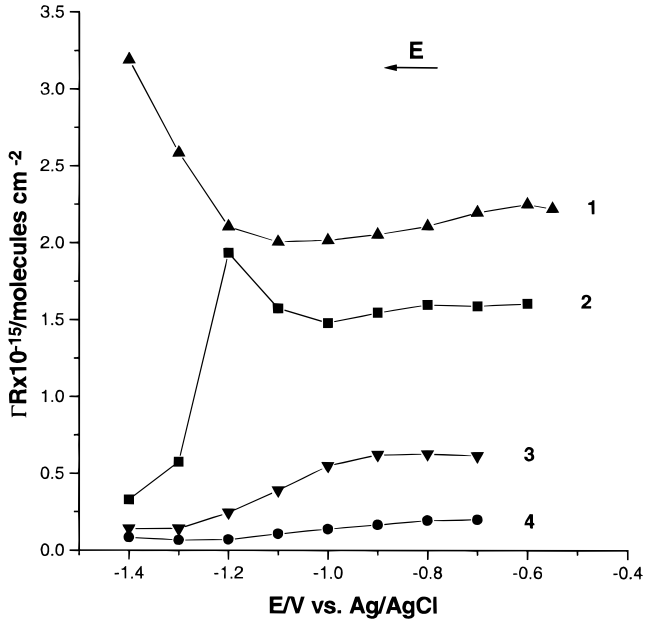

Figure 14. Radioactive labeling data. Potential dependence of sulfate sorption on Al 2024 during cathodic polarization in 0.1 M $NaClO_4$ at pH = 2.0 (curve 1), pH = 3.0 (curve 2), pH = 4.0 (curve 3), and pH = 10.0 (curve 4). $c_{sulfate}$ = 0.1 mM.

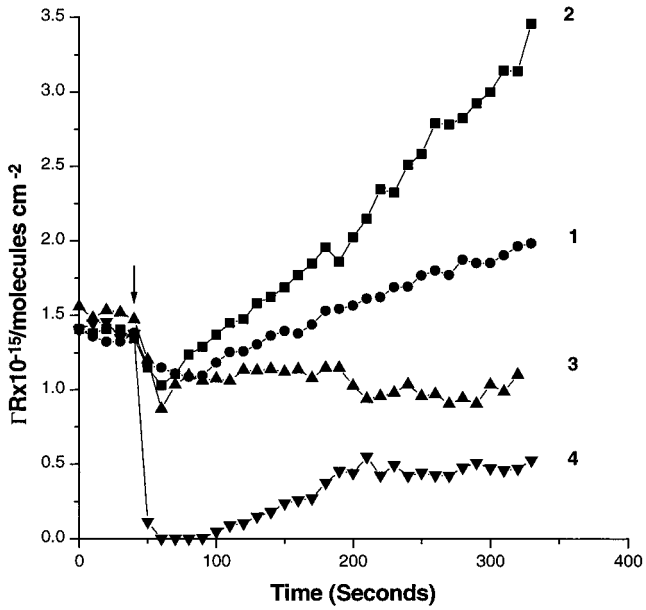

Figure 15. Radioactive labeling data. Kinetics of sulfate sorption on Al 2024 in 0.1 M $NaClO_4$ at pH = 3.0 after switching the potential from −0.70 V to −1.10 V (curve 1), to −1.20 V (curve 2), to −1.30 V (curve 3), and to −1.40 V (curve 4). $c_{sulfate}$ = 0.1 mM.

Aluminum ions are also released (at pH < 4.0; Figure 7) via a general dissolution mechanism.[31,35,36] Ultimately, the dissolved aluminum forms $Al(OH)_3$ that precipitates around the cathodic sites,[42,43] that is, on the copper-rich nodules (Figure 10C). When the appropriate pH conditions are met, the precipitate provides effective binding sites for sulfate adsorption (Figure 14, curve 1). The required low local pH value may be

(42) Shimizu, K.; Kobayashi, K.; Thompson, G. E.; Wood, G. C. *Corros. Sci.* **1993**, *34*, 1475.
(43) Brown, G. M.; Shimizu, K.; Kobayashi, K.; Thompson, G. E.; Wood, G. C. *Corros. Sci.* **1993**, *34*, 2099.

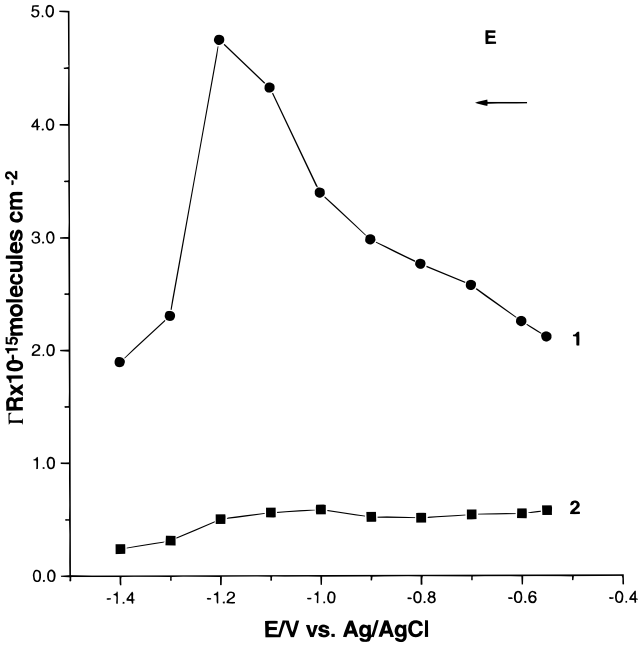

Figure 16. Radioactive labeling data. Potential dependence of sorption of sulfate (curve 1) and chloride (curve 2) on Al 2024 during cathodic polarization in 0.1 M $NaClO_4$ at pH = 3.0. $c_{sulfate}$ = 1 mM; $c_{chloride}$ = 1 mM.

predetermined by the correct balance between the rate of aluminum dissolution and the flux of protons to the surface. Due to the localized nature of the $Al(OH)_3$ formation, sulfate concentrates at the Cu-rich zones, as demonstrated in Figure 10E. In addition, when the bulk solution pH is close to neutral, the buffering capacity is low and the change in local pH is high. This results in decreasing sulfate adsorption with the negative-going polarization (Figure 14, curves 3 and 4). The dividing line between the two Γ vs *E* patterns is at pH = 3.0, as shown in Figure 14.

The morphological transformations observed at −1.40 V result from the destabilization of the oxide film by the hydrogen evolution reaction (Figure 11). The oxide removal also assists in anion desorption, as documented by the radioactive labeling data (curves 2−4 in Figure 14) and the SAM results (Figure 10F). Furthermore, the results given in Figures 12 and 14 imply that the availability of copper nodules at the appropriate pH determines the electrode potential threshold below which sulfate anion desorbs from the surface. Although the atomic concentration of copper on the surface increases, copper may have only an indirect effect on the anion deposition since no sulfate is adsorbed on copper at such negative potentials.[44] From these data, we conclude that sulfate is preferentially adsorbed on the aluminum oxide/hydroxide part of the surface rather than on copper-rich intermetallics where hydrogen evolution occurs. Collectively, these observations may explain the lack of effect of sulfate on the cathodic polarization curves demonstrated in Figure 9.

3. Practical Aspects of This Study. It appears from this study that that there is a significant buildup of adsorbed anions on the alloy surface under cathodic polarization (and protection) conditions. This may be detrimental for the stability of the alloy if a discontinuity or failure in cathodic protection occurs in an industrial environment. One plausible action scenario could be the following: the electrode potential control ends and the potential is shifted to more positive values, that is, toward the open-circuit potential. A fraction of anions accumulated during cathodic polarization may desorb, but most will remain entrapped at the surface or near surface zones.[45] Under such conditions, two requirements for accelerated local aluminum dissolution (localized corrosion) are met: a high anion surface concentration and potentials outside the cathodic protection range.[46,47] Therefore, care should be taken to apply the corrosion protection consistently. We also believe that more research is needed to check if other aluminum alloys are not subject to the concerns from above as is the Al 2024 alloy.

Conclusions

Sulfate and chloride anions investigated in this project are commonly present in chemical environments corrosive to the 2000 series of aluminum alloys. From this study, we may conclude that sorption of these anions on Al 2024 alloy is a complex interfacial event, involving oxidized and chemically heterogeneous surfaces, and two modes of anion−surface interaction: adsorption and incorporation. Whereas the adsorption processes are controlled by surface charge and the stability of the oxide films, the incorporation reflects the capability of the oxide to accommodate the anions during oxide growth, or its transformations in response to a pH and electrode potential change. In a comparative aspect, chloride adsorption is weaker than sulfate, and furthermore, the main part of the Cl^- adsorbate is incorporated in the surface oxide film. Undoubtedly, a combined effect of anionic charge, size, and hydration accounts for the difference, but more details are needed to enhance the interpretative strength of our data.

The spectroscopic and microscopic analysis of the surface of Al 2024 alloy revealed intrusions and extrusions (heterogeneities) containing enhanced amounts of Cu, Mg, Mn, and Fe. Since the heterogeneities play a clear role in the elemental and morphological transformations of the oxidized Al 2024 surface, they determine the stability of the alloy under electrochemical polarization conditions. We may conclude that the studied interfacial events are rarely two-dimensional and involve the micron-scale intermetallics embedded in aluminum matrixes, and many monolayers of oxide(s)/hydroxide(s) on the alloy surface. Clearly, corrosion of the Al 2024 alloy belongs to the category of electrochemical materials science rather than electrochemical surface science, including the effects of extensive roughening and a three-dimensional network formation through dissolution/precipitation processes. On the practical side, we have formulated a scenario in which cathodically accumulated anions may enhance the aluminum 2024 alloy corrosion. Namely, when the negative polarization (or cathodic protection) ends, the adsorbed anions are bound to be involved in a localized attack on the surface at a sufficiently positive electrode

(44) Rice-Jackson, L. M.; Horányi, G.; Wieckowski, A. *Electrochim. Acta* **1991**, *36*, 753.

(45) Kolics. A.; Polkinghorne, J. C.; Wieckowski, A., to be published.

(46) Atanasoska, Lj. D.; Drazic, D. M.; Despic, A. R.; Zalar, A. *J. Electroanal. Chem*. **1985**, *182*, 179.

(47) McCafferty, E. *Corros. Sci*. **1995**, *37*, 481.

potential. Overall, we believe our results offer a new perspective on the role of copper in the cathodic behavior of the Al 2024 alloy, and provide insights into intimate details of the anion adsorption/incorporation processes that accompany aluminum dissolution under cathodic polarization conditions.

Acknowledgment. This work was supported by the Department of Energy, Grant DEFG02-96-ER45439, administered by the Frederick Seitz Materials Research Laboratory at the University of Illinois and a grant provided by AEROVOX. Assistance from Nancy Finnegan (Auger electron spectroscopy), Rick Haasch (X-ray photoelectron spectroscopy) and Vania Petrova (scanning electron microscopy/EDAX) from Frederick Seitz Materials Research Laboratory is acknowledged. Auger electron, X-ray photoelectron spectroscopies and SEM studies were carried out in the Center for Microanalysis of Materials, University of Illinois, which is supported by the U.S. Department of Energy under Grant DEFG02-91-ER45439.

CM970603I